INTRAARTERIAL CONTRAST-ENHANCED COMPUTED TOMOGRAPHY OF THE EQUINE DISTAL EXTREMITY

SARAH M. PUCHALSKI, LARRY D. GALUPPO, WILLIAM J. HORNOF, ERIK R. WISNER

A technique for regional delivery of contrast medium to the foot of the horse to increase the diagnostic utility of computed tomography (CT) for the characterization of soft tissue structures within the hoof capsule was developed. An intraarterial catheter was placed under ultrasound guidance into the medial palmar artery at the level of the carpus to facilitate a steady-state infusion of iodinated contrast medium. Two 5 mm collimated contiguous acquisition CT scans were performed in 10 horses without lameness or radiographic evidence of distal sesamoid bone degeneration. CT examination was performed before and during regional arterial infusion of iodinated contrast medium administered at a rate of 2 ml/s. Cross-sectional area and mean pre- and post-contrast attenuation of the deep digital flexor tendon and the collateral ligaments of the distal interphalangeal joint were quantified from CT images. Soft tissue anatomy of the foot was also qualitatively characterized from pre-and postcontrast images. Catheterization was successful and without complication in all horses. The evaluated tendons and ligaments were clearly visible and had a small (8–20 Hounsfield Unit) but significant ($P < 0.05$, paired *t*-test) increase in attenuation during the steady-state infusion of contrast medium. This study should enhance the diagnostic potential of CT by providing baseline quantitative data for comparison with horses affected with soft tissue injuries in the distal extremity causing lameness that is alleviated with a palmar digital nerve block. *Veterinary Radiology & Ultrasound, Vol. 48, No. 1, 2007, pp 21–29.*

Key words: equine, contrast CT, distal extremity, lameness.

Introduction

ACCURATE DIAGNOSIS OF soft tissue injuries causing heel pain and lameness in horses is inhibited by a limited ability to examine the structures contained within the hoof capsule.[1,2] Diagnosis of tendon and ligament injury within the distal extremity has been augmented using magnetic resonance (MR) and ultrasound imaging. These modalities are useful adjuncts to physical examination, regional nerve blocks, and routine radiographic examination.[3–10] Nuclear scintigraphy has also shown clinical utility in the diagnosis of distal sesamoidean (navicular) remodeling and soft tissue insertional injuries.[11,12] The purpose of the current investigation is to introduce a technique for qualitative evaluation of the distal extremity and to define normal ranges for quantitative imaging parameters of clinically relevant soft tissue structures using contrast-enhanced computed tomography (CT).

From the Department of Surgical and Radiological Sciences, School of Veterinary Medicine, College of Veterinary Medicine, University of California, Davis, One Shields Avenue, Davis, CA 95616 (Puchalski, Galuppo, Wisner), Eklin Medical Systems Inc., 568 Weddell Dr., Suite 1, Sunnyvale, CA 94089 (Hornof)

Supported by the Center for Equine Health, UC Davis. The Center for Equine Health is supported with funds provided by the Oak Tree Racing Association, The State of California Pari-Mutuel Fund and contributions by private donors.

Address correspondence and reprint requests to Sarah M. Puchalski, at the above address. E-mail: wjhornof@ucdavis.edu

Received March 24, 2006; accepted for publication June 7, 2006.
doi: 10.1111/j.1740-8261.2007.00198.x

CT has value in the evaluation of osseous lesions but is also useful for the evaluation of tendon injury, particularly when the tendons are associated with complicated underlying osseous anatomy in regions such as the ankle.[13–20] CT is also used in peripheral musculoskeletal injury and in other sites of complex osseous anatomy such as the skull base.[18,21,22] In people, the utility of CT for the diagnosis of flexor tendon injury in the hand has increased through advances in three dimensional software.[23] In many imaging modalities, including CT, contrast medium administration through intrathecal and intravascular routes helps delineate soft tissues and soft tissue lesions that are otherwise difficult to identify.[24–29] It is also true that tendon healing is associated with hyperemia and increased vascularity of the surrounding soft tissue.[30–34] Therefore it is likely that intravascular administration of contrast medium would cause increased conspicuity of tendon and ligament injury in horses. However, the administration of an appropriate systemic dose of intravenous contrast medium in the horse is impractical due to the large volume and long administration time.[24,35]

There are few reports of specific applications of CT for the diagnosis of equine foot disorders. Conventional CT has been reported as less effective for diagnosis of soft tissue injury but slightly better than MR imaging for evaluation of bone within the foot.[36,37] Whereas many reports document the clinical utility of MR imaging for the diagnosis of tendon and ligament injuries within the hoof capsule, only two

reports describe the use of CT for the diagnosis of deep digital flexor tendon (DDFT) lesions.[4–7,9,38,39]

The objective of this study was to develop a technique for regional administration of iodinated contrast medium to the equine distal extremity and to quantify normal values for tendon and ligament cross-sectional area and attenuation before and after contrast medium administration as well as and qualitatively characterize the anatomy of the foot on contrast-enhanced CT images. It is anticipated that contrast-enhanced CT would provide a unique method for diagnosing soft tissue lesions within the hoof capsule of the equine distal extremity.

Materials and Methods

Six Thoroughbred and four Warmblood breed horses between 4 and 12 years of age and weighing 350–500 kg were studied. A cursory lameness examination including jogging on a circle and in a straight line on hard ground was performed the same day as the imaging procedure and to be studied the horse had to have no lameness in the imaged limb. All horses had routine distal extremity radiographic examination that included a lateromedial, a dorsal 45° proximal to palmarodistal oblique, a dorsal 65° proximal to palmarodistal oblique navicular cone down view, a dorsal 65° proximal to palmarodistal oblique, and a palmaro 85° proximal to palmarodistal oblique performed the day before or the day of the CT exam. Horses were excluded if radiographic findings of distal sesamoidean medullary sclerosis, proximal border entheses formation, distal border fragmentation, palmar cortical destruction, or alterations in bone shape were evident. Horses with fewer than five synovial invaginations measuring less than 3 mm in diameter were included in the study. In each horse only one forelimb was used. Left and right forelimbs were alternated in successive horses.

Technique

Each horse was sedated using xylazine (0.5–1.0 mg/kg, intravenously [IV]) as a premedication, and a combination of ketamine (1 mg/kg, IV) and diazepam (0.05 mg/kg, IV) for induction of anesthesia. General anesthesia was maintained with inhaled isoflurane and oxygen. Each horse was positioned in lateral recumbency on a custom built CT table* with the dependent forelimb centered within the CT gantry†.

The selected forelimb was positioned so that the longitudinal axis of the limb was oriented parallel to the table and perpendicular to the plane of the CT gantry. The dependent limb position was maintained using foam pads for support and adhesive tape. In initial studies, three aluminum rods were taped to the outside of the digit to serve as external fiducial markers. These produced a slight high-density edge gradient artifact on CT images and hollow plastic rods were used for subsequent studies.

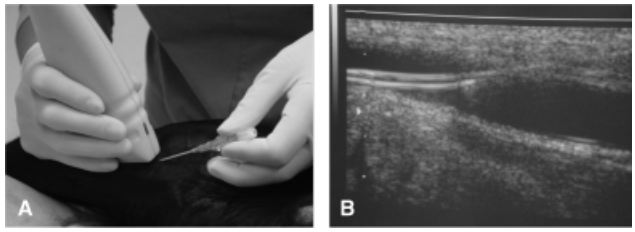

FIG. 1. (A) A linear 10–5 MHz ultrasound probe is used to guide an 18 gauge × 48 mm long intravenous catheter into the medial palmar artery at the distal aspect of the carpus of a right limb. (B) Gray scale ultrasound image showing the catheter crossing through the soft tissues into the lumen of the medial palmar artery.

Once the limb was positioned, the distomedial aspect of the carpus was clipped and aseptically prepared for catheter insertion. An 18 gauge × 1.88 in. catheter (1.8 × 48 mm)‡ was introduced into the medial palmar artery with ultrasonographic guidance using a 10–5 MHz blended linear probe§ (Fig. 1A and B). The medial palmar artery was consistently identified deep and slightly palmar to the medial palmar vein and deep to the flexor retinaculum of the carpus. These structures were identifiable and were avoided using ultrasound guidance. Once the catheter was placed, it was affixed to the skin using polypropylene suture¶. A capped three-way stopcock was then attached to the catheter to facilitate contrast medium injection. A remote controlled pressure injector‖ was then attached to the catheter by two (inline) 34 in. extension sets.# The pressure injector and extension sets were prefilled with ionic-iodinated contrast medium** diluted 1:1 with normal saline (0.9% NaCl).

All horses were maintained on positive pressure ventilation for the duration of the anesthesia. Immediately before each CT scan all horses were hyperventilated and then the ventilator was turned off for the scan producing a breath hold to minimize patient respiratory motion during the 45–60 s scan.

At the conclusion of each imaging study, the intraarterial catheter was removed, a pressure bandage was applied to the carpus and the horses were moved to a recovery stall and recovered from anesthesia in a routine fashion. Each horse was monitored for 24 h for any complication of the procedure or anesthesia.

CT Scanning Protocol

In all horses two helical CT scans were performed. Three of the 10 horses had an additional CT scan performed. The

*Kimsey Corp., Woodland, CA.
†HiSpeed FX/I, GE Medical System Milwaukee, WI.
‡BD Angiocath™, BD Franklin Lakes, NJ.
§ATL 5000, Phillips Medical Systems, Bothell, WA.
¶2-0 PROLENE™, Ethicon Inc., Somerville, NJ.
‖MEDRAD Vistron CT, MEDRAD Inc., Indianola, PA.
#Baxter Healthcare Corp., Deerfield, IL.
**RenoCal-76, Bracco Diagnostics, Princeton, NJ.

first study ($CT_{precontrast}$) was comprised of 5 mm contiguous images from the mid portion of the proximal phalanx to the distal extent of the distal phalanx including the distal lamina. The second study ($CT_{postcontrast}$) was a repeat of the first during which a continuous arterial infusion of contrast medium was administered at 2 ml/s, beginning 3 s before the initiation of the CT exam. The infusion continued for the duration of image acquisition.

The third study, obtained in the final three subjects, consisted of 1 mm slices through the navicular bone (NB) and insertion of the DDFT and distal sesamoidean impar ligament (DSIL) on the distal phalanx. This study was performed without contrast medium after the previously described imaging acquisitions. The data collected from this sequence were used to reformat images in a sagittal plane using a multiplanar reformat tool available on viewing software†† in an attempt to better visualize the insertion points of the soft tissue structures.

For all imaging sequences, the tube output parameters were 120 kVp of and 150 mA. One-second helical images were obtained using a pitch of one and a gantry tilt of zero. All images were reconstructed with a soft tissue algorithm using a 17.4 × 17.4 cm defined field of view and a 512 × 512 pixel matrix. The 5 mm precontrast and postcontrast CT scans generated 30–35 images dependent on the size of the horse. The 1 mm scan generated 20–25 images.

Image Analysis

Image analysis was performed on a diagnostic imaging viewing station configured with a 1900 × 1250 pixel flat screen monitor.‡‡ Quantitative measurements of cross-sectional area and mean attenuation were obtained using custom software written in Matlab 6.0.§§

Quantitative measurements of cross-sectional area and mean attenuation of the DDFT and the collateral ligaments of the distal interphalangeal joint (DIPCL) were performed using operator-defined region-of-interest (ROI) analysis on the $CT_{precontrast}$ images viewed using a window of 200–400 Hounsfield units (HUs) and a level of 40–100 HU. Qualitative evaluation of the distal sesamoid (navicular) bone was also performed on this run using a window of approximately 2000 HU and a level of 750 HU. The NB was evaluated qualitatively for cortical and trabecular bone definition and synovial invaginations.

Qualitative assessment of the DDFT and DIJCLs, the distal digital sheath (DS), the collateral sesamoidean ligaments (CSL), the DSILs, the distal sesamoid bone (NB), and the podotrochlear (navicular) bursa was performed on this image set. The structures were evaluated for visibility and graded on a scale of 0–2 (0 = not visible, 1 = visible, and 2 = excellent visualization). Mean values and standard deviation for visibility score were calculated for each structure. Descriptors also included shape, homogeneity, and symmetry with the same structure on the opposite side of the limb (DIJCLs and the CSL) or within the same structure (DDFT).

$CT_{postcontrast}$ was used to quantify the degree of contrast enhancement in the DDFT and the DIJCLs and to describe the pattern of contrast enhancement. These images were evaluated using a window of approximately 200–400 HU and a level of 40–100 HU.

The third set of noncontrast 1 mm images, were reformatted into a sagittal plane using a multiplanar reformat tool available on viewing software,††. The reformatted images were evaluated qualitatively to define the size, shape, and homogeneity of the insertion of the DDFT and the DSIL. The visibility scoring system of 0–2 (0 = not visible, 1 = visible, 2 = excellent visibility) was applied to the DDFT insertion and the impar ligament insertion using these images.

ROI were drawn manually on the precontrast images that followed the external surface of the DDFT at three specified locations (Figs. 2–4) and the DIPCL at one location (Fig. 5). The DDFT measurements were made at the level of the proximal interphalangeal joint (DDFT 1); at the middle of the middle phalanx (DDFT 2), and proximal to the NB (DDFT 3). The images were aligned using the fiducial markers. Once the ROIs were drawn and the pre- and postcontrast images were aligned, the software program calculated mean HU per pixel for the ROI on both sets of images. Cross-sectional area was calculated based on the number of pixels, the pixel matrix, and the defined field of view.

Data Analysis

Descriptive statistics were used to evaluate the results. A paired *t*-test with a *P*-value of less than 0.05 was used to determine statistical significance of the increase in HU after contrast medium administration.

Results

Arterial catheterization was successful in all horses. The medial palmar artery was readily identifiable in all horses, deep and slightly palmar to the medial palmar vein and deep to the carpal flexor retinaculum. Initially, the catheter was placed approximately at the level of the accessory carpal bone. At this location, the catheter was placed through the retinaculum causing it to be partially occluded, making injection difficult. Placing the catheter distal to the retinaculum at approximately the level of the carpometacarpal joint alleviated this problem. The first branch of the medial palmar artery, a communicating artery to the lateral

††eFilm, Merge Healthcare, Milwaukee, WI.

‡‡SyncMaster 240 T, Samsung Electronics Co., Ltd., Ridgefield Park, NJ.

§§The Mathworks Inc., Natick, MA.

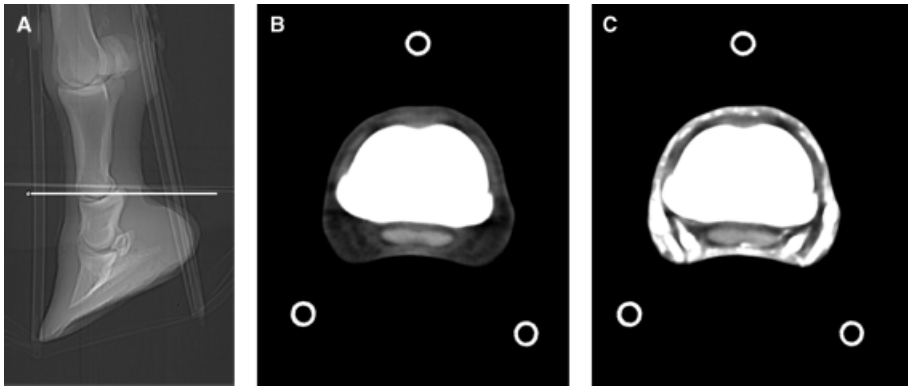

FIG. 2. (A) Scout image with localizer marker at the level of the proximal interphalangeal joint demonstrating the level of the region denoted by deep digital flexor tendon (DDFT) 1. (B) Precontrast 5 mm transverse image (window = 200, level = 100) of the pastern at DDFT 1 showing the DDFT within the digital sheath. (C) Postcontrast 5 mm transverse image (window = 200, level = 100) at DDFT 1. The increase in attenuation (Hounsfield unit) after contrast medium administration is not perceptible without quantification. The DDFT is well demarcated, the digital sheath is a thin, hypoattenuating structure surrounding the tendon.

palmar artery, could be identified using ultrasound and the catheter was placed proximal to this branch. On one occasion, the catheter was placed in the communicating branch to the lateral arterial vasculature. The catheter was replaced more proximally and the infusion was not compromised. In all instances of initial catheter misplacement, pressure was applied to the initial catheter site and a second catheter was repositioned in the appropriate location. No horse developed any complication related to catheter placement and subsequent removal and catheter misplacement did not hinder placement of an additional catheter.

DDFT—Precontrast

The DDFT was readily identifiable from the distal pastern to the level of the distal NB. The DDFT was smoothly margined and the margins were clearly demarcated. Proximal to the NB, the tendon had a distinctly bilobed appearance with both lobes being symmetric in size and shape. As the tendon approached the NB, it flattened in a dorsopalmar direction with the bilobed appearance becoming less distinct and the dorsopalmar distance reduced as it inserts onto the distal phalanx. The DDFT distal to the NB was difficult to delineate from the DSIL on the 5 mm axial images. On all three of the sagitally reformatted 1 mm images, the DDFT and the impar ligament were clearly demarcated by a hypoattenuating stripe between them (Fig. 6A and B). The attenuation of the DDFT was homogeneous throughout its length. Visibility of the DDFT at the three defined locations, DDFT 1–3, were all scored as a mean $\pm$ SD of 2 ± 0. At the insertion the score was 1 ± 0. On the sagitally reformatted images the DDFT insertion was scored as 2 ± 0.

DDFT—Postcontrast

After contrast medium administration, there was a slight but statistically significant increase in attenuation

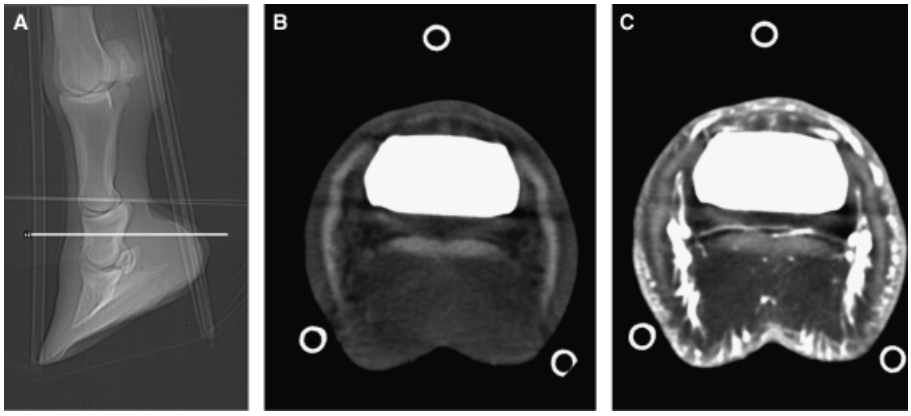

FIG. 3. (A) Scout image with localizer marker at the middle of the middle phalanx demonstrating the level denoted by deep digital flexor tendon (DDFT) 2. (B) Precontrast 5 mm transverse image (window = 200, level = 100) of the distal pastern at DDFT 2. (C) Postcontrast 5 mm transverse image at the same level as (B). The ungual cartilages, the proximal portion of the navicular bursa, the collateral sesamoidean ligaments, the DDFT and the distal portion of the digital sheath are visible.

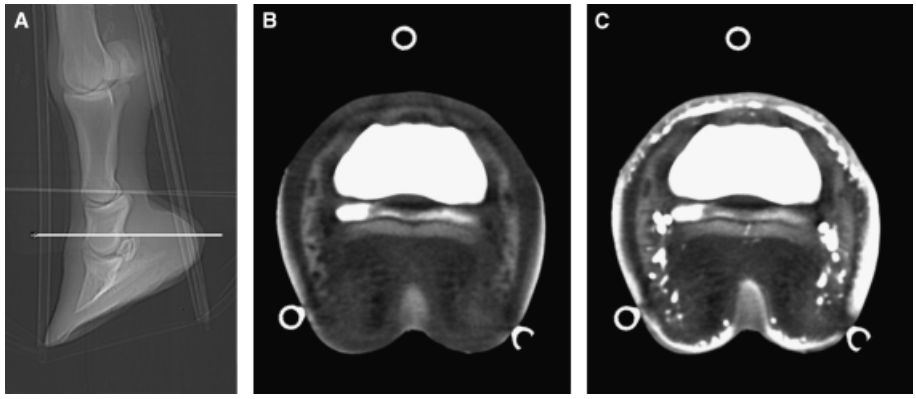

FIG. 4. (A) Scout image with the localizer marker at the proximal border of the navicular bone demonstrating the level denoted by deep digital flexor tendon (DDFT) 3. (B) Precontrast 5 mm transverse image (window = 200, level = 100) at the proximal aspect of the navicular bone. (C) Postcontrast 5 mm axial image at the same level as (B). The DDFT flattens as it passes over the palmar surface of the navicular bone and bursa. Volume averaging causes the navicular bone to appear incomplete on these axial images. The ungual cartilages and the proximal aspects of the distal interphalangeal collateral ligaments are visible.

of the DDFT ranging from 8 to 17 HU (Table 1, $P < 0.05$). The DDFT maintained a homogenous pattern of attenuation after contrast medium administration at DDFT 1–3. At the level of the NB, where the DDFT curves over the flexor cortex of the bone, small blood vessels were visible in the palmar surface of the DDFT (Fig. 5C).

DIPCL—Precontrast

The DIPCLs were readily identifiable and appeared symmetric in size and shape. The ligaments were smoothly margined but became less so proximal to their insertions. The ligaments maintained a rectangular to ovoid shape through their mid bodies. Measurement of the collateral ligaments was highly repeatable (Fig. 5, Table 2). The ligaments had a homogeneous attenuation pattern. Visibility of the DIJCLs was scored as 1.5 ± 0.5 at the origin, 1.8 ± 0.4 at their mid body, and 2.0 ± 0 at their insertion onto the distal phalanx.

DIPCL—Postcontrast

After contrast medium administration, the collateral ligaments also had a small but statistically significant increase in relative attenuation averaging 12 HU (Fig. 5A and B, Table 1, $P < 0.05$). The DIPCL had a homogenous attenuation pattern after contrast medium administration.

DS

The DS extended distally within the foot for a variable distance in different horses. In all of the normal horses, the DS was visible and appeared as a thin hypoattenuating stripe surrounding the DDFT (Figs. 2A and 3A). It was generally well defined but became smaller as it approached the proximal extent of the podotrochlear bursa. The visibility of the DS was scored as 1.2 ± 0.4.

Podotrochlear (Navicular) Bursa

The proximal recess of the navicular bursa was identifiable as a hypoattenuating structure just proximal to the

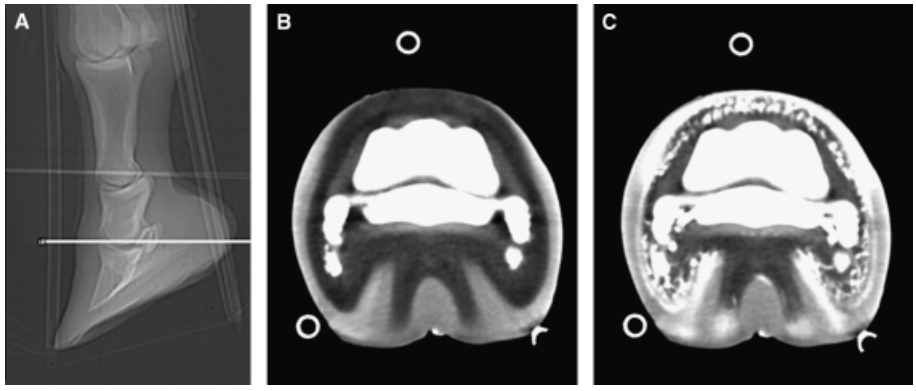

FIG. 5. (A) Scout image with the localizer marker at the level of the distal interphalangeal joint demonstrating the level of mid body of the distal interphalangeal collateral ligaments (DIPCL). (B) Precontrast 5 mm transverse image (window = 200, level = 100) through the distal interphalangeal joint. (C) Postcontrast 5 mm axial image at the same level of (B). The DIPCLs are well demarcated and symmetric.

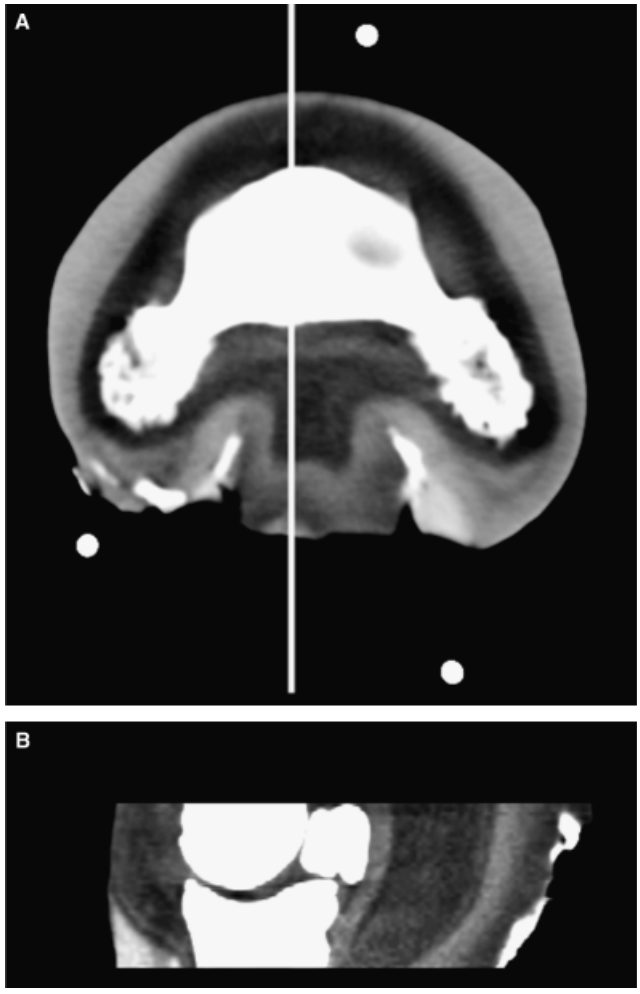

FIG. 6. (A) 1 mm transverse image of the deep digital flexor tendon (DDFT) distal to the distal sesamoid bone. The localizer marker demonstrates the orientation of the multiplanar reformat tool. (B) Sagitally reformatted image of the insertion of the DDFT and the distal sesamoidean impar ligament. A thin, hypoattenuating stripe is present between the two structures distal to the distal sesamoid bone.

NB, dorsal to the distal portion of the DS. At its proximal extent the bursa scored had a visibility score of 1.4 ± 0.5. The bursa was poorly visible over the flexor surface of the NB (Fig. 4B) with a visibility score of 0 ± 0.

Distal Sesamoid NB

In all horses, the NB had good corticomedullary definition and multiple small synovial invaginations in the distal border. On the 1 mm images bone detail was excellent allowing for evaluation of the dorsal articular border and flexor cortex (Fig. 7), insertion of the CSL and the origin of the DSIL.

DSIL

The impar ligament was poorly visualized on the axial images with a visibility score of 0.1 ± 0.3. It was seen on the sagittal plane reformatted 1 mm images as a homogeneous thin stripe dorsal to the DDFT with attenuation similar to the DDFT (Fig. 6) and a score of 1 ± 0. A value for relative attenuation was not obtained due to the difficulty in visualization on the 5 mm axial slices.

CSLs

The CSLs were seen on axial images as roughly triangular structures extending from the proximal aspect of the medial and lateral extremities of the NB to the palmar aspect of the middle phalanx, visibility score was 1.5 ± 0.5. The small size of the ligaments coupled with relatively thick slices made volume averaging a factor such that relative attenuation was not obtained for these paired structures.

Discussion

In this study a technique for the regional administration of iodinated contrast medium to the foot of the horse is described. In addition to the technique, normal values for tendon and ligament attenuation before and after contrast medium administration were determined and a qualitative description of the anatomy of the foot on CT images was developed. This technique was developed to use the properties of intravascular contrast medium and tendon healing to increase tendon lesion conspicuity within the hoof capsule.

Ultrasound guided arterial catheterization is a key component of this technique. In all horses, arterial catheterization was successful and relatively quick to perform. Catheterization did not result in associated complications

TABLE 1. Attenuation of the Deep Digital Flexor Tendon (DDFT) and the Medial and Lateral Distal Interphalangeal Collateral Ligaments (MCL, LCL) Before and After Intra-Arterial Administration of Iodinated Contrast Medium

Location	PreContrast Attenuation (HU)	Standard Deviation	PostContrast Attenuation (HU)	Standard Deviation	Change (HU)	*P*-Value
DDFT 1	123	6.3	134	9.3	11*	0.0003
DDFT 2	96	6.0	104	7.5	8*	0.0002
DDFT 3	110	6.5	127	7.7	17*	0.01
MCL	75	5.7	87	8.4	12*	0.02
LCL	70	5.7	82	10.1	12*	0.02

*Significant increase paired *t*-test ($P < 0.05$).

TABLE 2. Cross-Sectional Area of the Deep Digital Flexor Tendon (DDFT) at Three Locations and the Medial and Lateral Collateral Ligaments (MCL, LCL) of the Distal Interphalangeal Joint

Location	Mean (cm^2)	Standard Deviation (cm^2)
DDFT 1	0.441	0.024
DDFT 2	0.661	0.135
DDFT 3	0.531	0.170
MCL	0.322	0.050
LCL	0.360	0.050

DDFT 1, at the level of the proximal interphalangeal joint; DDFT 2, at the middle of the middle phalanx; DDFT 3, at the proximal aspect of the navicular bone.

in any horse. The two major encumbrances associated with catheter placement included the carpal flexor retinaculum, and placement of the catheter in the communicating branch of the medial palmar artery. These structures can be avoided, as they are both visible through ultrasound evaluation of the regional anatomy.

Qualitative and quantitative evaluation of the DDFT and the collateral ligaments indicated that normal tendon and ligament morphology should be of uniform attenuation with medial to lateral symmetry. These findings were similar to the morphologic evaluation of the same structures using MR imaging.[9] In all horses, the borders of the DDFT were clearly demarcated and smooth proximal to and at the level of the NB. This appearance was lost through the level of the insertion of the tendon, which was likely in part due to the oblique plane of sectioning as the tendon passes between the distal aspect of the NB and the distal phalanx. Decreasing the slice thickness and using multiplanar reformatting tools improved visualization of the DDFT insertion.

Cross-sectional area measurements of the DDFT have been reported previously[9] however a comparison between the two studies is difficult to make. Measurements were not made at the same anatomic location and there is documented size change of the tendon depending on the level at which it is measured. It is therefore reasonable to have discrepancy between the values reported for the same anatomic structure. Additionally, because of the nature of CT image acquisition, the transverse images are perpendicular to the hoof wall, which generally yields an image perpendicular to the long axis of the DDFT in the pastern region but a slightly oblique image as the tendon curves. This obliquity would cause the cross-sectional area measurement to be slightly erroneous. Further, partial volume averaging is a factor that likely plays a role in decreasing measurement accuracy. Although these potential errors exist, the reported measurements are likely useful if limb positioning and imaging techniques are similar. An important and congruous finding was the previously documented[9] medial to lateral symmetry of the DDFT itself.

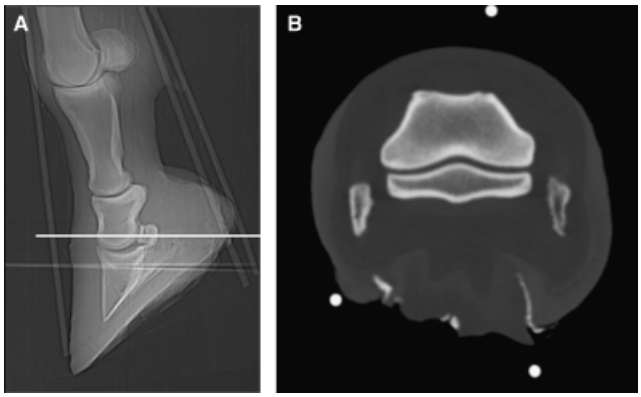

FIG. 7. (A) Scout image with the localizer marker at the level of the navicular bone and distal aspect of the middle phalanx. (B) Precontrast 5 mm transverse image through the distal middle phalanx, distal sesamoid bone and the palmar processes of the distal phalanx. The window and level have been adjusted for better evaluation of bone (window = 2000, level = 750).

In addition to the DDFT and collateral ligaments, some of the smaller soft tissue structures were identifiable in all horses. These included the distal sesamoidean collateral ligaments, DSIL, and proximal aspect of the podotrochlear bursa and the distal extent of the DS. Evaluation of these structures was performed on both the pre- and the postcontrast studies and a change in their appearance was not observed. Damage and particularly inflammation of these structures is anticipated to cause contrast enhancement leading to the identification of abnormalities of these smaller structures. Multiplanar reformatting enabled visualization of the insertion of the impar ligament and the DDFT. Although the dorsal to palmar thickness of the distal portions of the DDFT and the DSIL were not quantified, a thin hypoattenuating stripe was present on the reformatted images. It is likely with injury at these sites, increases in cross-sectional area through tendon and ligament swelling will cause this stripe to be lost.

Rapid, helical scanning is also essential to the technique reported herein. Each of the imaging acquisitions was completed within 30–45 s. This enabled the contrast medium infusion to be performed simultaneously with image acquisition. It also produces high quality reformatted images giving a better anatomic depiction of the most distal portion of the foot. Furthermore, because respiratory motion has the potential to cause enough distal limb motion to degrade image quality, the fast acquisitions could be performed during a single breath hold.

During the infusion of contrast medium both the DDFT and the DIPCL had a small, but statistically significant increase in attenuation measured in HUs. The maximum value for enhancement of any structure was 20 HU. The degree of contrast enhancement is small and this degree of enhancement was nearly imperceptible without quantification. To provide a meaningful quantification of DDFT attenuation, care must be taken to exclude vasculature lo-

cated along its dorsal border as the tendon approaches the NB and the distal extent of the CS (Fig. 3B and C). Similarly, the laminar blood vessels must be avoided in quantifying the attenuation of the DIJCLs (Fig. 5B and C). Documentation of baseline enhancement is likely important for diagnosing lesions within tendinous and ligamentous structures using contrast-enhanced CT.

There are a limited number of reports describing the use of CT for evaluation of the distal extremity in horses and one report describing the vascular anatomy of the foot using CT angiography.[36–39] In two reports, CT was reported as having excellent detail in the evaluation of bone structure, but poor delineation of the soft tissues.[36,37] With appropriate window and leveling of the acquired CT images, the soft tissue anatomy was well defined, in addition to the excellent bone detail expected from CT. This has been shown to be true in imaging for injuries to the human ankle (Achilles and peroneus brevis) tendons.[14,15,17,19,20,30] CT has been used specifically for the evaluation of the DDFT within the foot and changes in attenuation and size are identified in lesions of the DDFT.[38,39] In one report, injured tendons had decreased attenuation when compared to the more normal tendon surrounding the lesion.[38] With the baseline information developed in this study, aberration from the expected attenuation can be recognized by comparing absolute values in HU.

After tendon injury, healing occurs in three overlapping phases. In the initial phase vasoactive and chemotactic factors are released that increase vascular permeability, initiate angiogenesis, stimulate tenocyte proliferation, and recruit more inflammatory cells. In the intermediate phase increased water and glycosaminoglycan concentration remain high. In the remodeling phase, repair tissue changes from cellular to fibrous.[33] Throughout tendon healing, alterations in the pattern of intravascular contrast enhancement of tendons are expected through changes in tissue permeability and neovascularization and should be identifiable using contrast-enhanced CT. Vascular in growth and tendon hyperemia is documented in people with Achilles and patellar tendinopathy on histopathology through power Doppler imaging.[30–34] Using a simultaneous intravascular contrast medium infusion and CT scanning regions with new blood vessels are expected to be visible. It is further expected that injured tendons will enhance beyond the expected value of 10–20 HU increasing the confidence of the image interpreter in the diagnosis of tendinopathy.

Although MRI is generally considered the mainstay of orthopedic imaging, some limitations of the modality and its use in equine veterinary medicine exist. Even though MRI is becoming more commonplace, lack of availability is still a problem in many hospitals. Further, if CT is present at a hospital then MRI may not be available on a routine basis and it is possible that only one modality is present. This technique should provide a means of increasing the diagnostic utility of CT. The commonly touted limitation of MRI and bone imaging is that there is decreased anatomic detail of osseous structures and that CT maintains superiority in the evaluation of bone morphology. Therefore, CT may have improved diagnostic capabilities when evaluating bone change. The introduction of contrast medium improves anatomic CT imaging by providing a means of evaluating the underlying physiology, which in turn should increase the utility of CT for soft tissue lesion diagnosis.

In this study, a technique for the local delivery of contrast medium to the foot, normal quantitative parameters of cross-sectional area, and attenuation of the DIPCL and the DDFT before and during contrast medium delivery were described. A small, statistically significant increase in attenuation was identified in all soft tissues evaluated. Qualitative parameters of the soft tissues of the foot were also described. Further investigation using contrast-enhanced CT is necessary to evaluate its clinical utility for the identification of soft tissue injuries causing lameness in horses.

REFERENCES

1. Ross M, Dyson S. Diagnosis and management of lameness in the horse, 1st ed. Philadelphia: W.B. Saunders, 2002.
2. Adams OR, Stashak T. Adam's lameness in the horse, 5th ed. Philadelphia: Lippincott, Williams and Wilkins, 2002.
3. Denoix JM. Diagnostic techniques for identification and documentation of tendon and ligament injuries. Vet Clin North Am Equine Pract 1994;10:365–407.
4. Dyson SJ, Murray RC, Schramme MC, et al. Lameness in 46 horses associated with deep digital flexor tendonitis in the digit: diagnosis confirmed with magnetic resonance imaging. Equine Vet J 2003;35:681–690.
5. Dyson SJ, Murray RC, Schramme MC, et al. Magnetic resonance imaging of the equine foot: 15 horses. Equine Vet J 2003;35:18–26.
6. Dyson SJ, Murray RC, Schramme MC, et al. Collateral desmitis of the distal interphalangeal joint in 18 horses (2001–2002). Equine Vet J 2004;36:160–166.
7. Dyson SJ, Murray R, Schramme MC. Lameness associated with foot pain: results of magnetic resonance imaging in 199 horses (January 2001–December 2003) and response to treatment. Equine Vet J 2005;37:113–121.
8. Kleiter M, Kneissl S, Stanek C, et al. Evaluation of magnetic resonance imaging techniques in the equine digit. Vet Radiol Ultrasound 1999;40:15–22.
9. Murray RC, Roberts BL, Schramme MC, et al. Quantitative evaluation of equine deep digital flexor tendon morphology using magnetic resonance imaging. Vet Radiol Ultrasound 2004;45:103–111.
10. Widmer WR, Buckwalter KA, Hill MA, et al. A technique for magnetic resonance imaging of equine cadaver specimens. Vet Radiol Ultrasound 1999;40:10–14.
11. Trout DR, Hornof WJ, O'Brien TR. Soft tissue and bone phase scintigraphy for diagnosis of navicular disease in horses. J Am Vet Med Assoc 1991;198:73–77.
12. Dyson SJ. Subjective and quantitative scintigraphic assessment of the equine foot and its relationship with foot pain. Equine Vet J 2002;34:164–170.
13. Rosenberg Z, Feldman F. Intra-articular calcaneal fractures: CT analysis. Skeletal Radiol 1987;16:105–113.
14. Rosenberg ZS, Feldman F, Singson RD, et al. Ankle tendons. Evaluation with CT. Radiology 1988;166:221.

15. Rosenberg Z, Feldman F, Singson R. Peroneal tendon injuries: CT analysis. Radiology 1986;161:743–748.

16. Kalebo P, Goksor L, Sward L, et al. Soft- tissue radiography, computed tomography and ultrasonography of partial Achilles tendon ruptures. Acta Radiol 1990;31:565–570.

17. Keyser CK, Gilula LA, Hardy DC, et al. Soft tissue abnormalities of the foot and ankle. CT diagnosis. Am J of Roentgenol 1988;150:845.

18. Lazarus M. Imaging of the foot and ankle in the injured athlete. Med Sci Sports Exerc 1999;317 (Suppl):S412–S420.

19. Rosenberg Z, Cheung Y, Jahss M. Computed tomography scan and magnetic resonance imaging of ankle tendons: an overview. Foot Ankle 1988;8:297–307.

20. Szczukowski M, St.Pierre R, Fleming L. CT evaluation of peroneal tendon dislocation: a report of 2. Am J Sports Med 1983;11:444–447.

21. Kraus DH, Lanzieri CF, Wanamaker JR, Little JR, Lavertu P. Complementary use of computed tomography and magnetic resonance imaging in assessing skull base lesions. Laryngoscope 1992;102:623–629.

22. Bohndorf K, Kilcoyne R. Traumatic injuries: imaging of peripheral musculoskeletal injuries. Eur Radiol 2002;12:1605–1616.

23. Sunagawa T, Ochi M, Ishida O, et al. Three-dimensional CT imaging of flexor tendon ruptures in the hand and wrist. J Comput Assist Tomogr 2003;27:169–174.

24. Yochum TR, Kettner NW, Barry MS, et al. Diagnostic imaging of the musculoskeletal system. In: Yochum RL, T R (eds): Yochum and Rowe's essentials of skeletal radiology. Baltimore, MD: Lippincott Williams and Wilkins, 2005;485–678.

25. Charousset C, Bellaiche L, Duranthon LD, et al. Accuracy of CT arthrography in the assessment of tears of the rotator cuff. J Bone Jt Surg 2004;87B:824–828.

26. Banfield CM, Morrison WB. Magnetic resonance arthrography of the canine stifle joint: technique and applications in eleven military dogs. Vet Radiol Ultrasound 2000;41:200–213.

27. Rowan KR, Keogh C, Andrews G, et al. Essentials of shoulder MR arthrography: a practical guide for the general radiologist. Clin Radiol 2004;59:327–334.

28. Samii VF, Dyce J. Computed tomographic arthrography of the normal canine stifle. Vet Radiol Ultrasound 2004;45:402–406.

29. vanBree H, Van Ryssen B, Degryse H, et al. Magnetic resonance arthrography of the scapulohumeral joint in dogs, using gadopentetate dimeglumine. Am J Vet Res 1995;56:286–288.

30. Campbell RS, Grainger AJ. Current concepts in imaging of tendinopathy. Clin Radiol 2001;56:253–267.

31. Kristoffersen M, Ohberg L, Johnston C, et al. Neovascularisation in chronic tendon injuries detected with colour Doppler ultrasound in horse and man: implications for research and treatment. Knee Surg Sports Traumatol Arthrosc 2005;13:505–508.

32. Newman JS, Alder RS, Bude RO, et al. Detection of soft tissue hyperemia: value of power Doppler sonography. Am J Roentgenol 1994;163:385–389.

33. Sharma P, Maffulli N. Tendon injury and tendinopathy: healing and repair. J Bone Jt Surg 2005;87:187–202.

34. Weinberg E, Adams M, Hollenberg G. Color Doppler sonography of patellar tendinosis. Am J of Roentgenol 1998;171:743–744.

35. Tidwell A, Jones J. Advanced imaging concepts: a pictorial glossary of computed tomography and magnetic resonance imaging. Clin Tech Small Anim Pract 1999;14:65–111.

36. Whitton RC, Buckley C, Donovan T, et al. The diagnosis of lameness associated with distal limb pathology in a horse: a comparison of radiography, computed tomography and magnetic resonance imaging. Vet J 1998;155:223–229.

37. Widmer WR, Buckwalter KA, Fessler JF, et al. Use of radiography, computed tomography and magnetic resonance imaging for evaluation of navicular syndrome in the horse. Vet Radiol Ultrasound 2000;41:108–116.

38. Nowak M. The Role of DDFT Tendinitis in Navicular Syndrome—a CT Perspective. In 1st World Orthopaedic Veterinary Congress. 2002. Munich.

39. Tietje S, Nowak M, Petzoldt S, et al. Computed tomographic evaluation of the distal aspect of the deep digital flexor tendon in horses. Pferdheilkunde 2001;17:21–29.